Atmos. Chem. Phys., 11, 13029–13045, 2011
www.atmos-chem-phys.net/11/13029/2011/
doi:10.5194/acp-11-13029-2011

Atmospheric Chemistry and Physics

Trends of solar ultraviolet irradiance at Barrow, Alaska, and the effect of measurement uncertainties on trend detection

G. Bernhard

Biospherical Instruments, San Diego, California, USA

Received: 22 July 2011 – Published in Atmos. Chem. Phys. Discuss.: 26 September 2011
Revised: 3 December 2011 – Accepted: 8 December 2011 – Published: 21 December 2011

Abstract. Spectral ultraviolet (UV) irradiance has been observed near Barrow, Alaska (71° N, 157° W) between 1991 and 2011 with an SUV-100 spectroradiometer. The instrument was historically part of the US National Science Foundation's UV Monitoring Network and is now a component of NSF's Arctic Observing Network. From these measurements, trends in monthly average irradiance and their uncertainties were calculated. The analysis focuses on two quantities, the UV Index (which is affected by atmospheric ozone concentrations) and irradiance at 345 nm (which is virtually insensitive to ozone). Uncertainties of trend estimates depend on variations in the data due to (1) natural variability, (2) systematic and random errors of the measurements, and (3) uncertainties caused by gaps in the time series. Using radiative transfer model calculations, systematic errors of the measurements were detected and corrected. Different correction schemes were tested to quantify the sensitivity of the trend estimates on the treatment of systematic errors. Depending on the correction method, estimates of decadal trends changed between 1.5 % and 2.9 %. Uncertainties in the trend estimates caused by error sources (2) and (3) were set into relation with the overall uncertainty of the trend determinations. Results show that these error sources are only relevant for February, March, and April when natural variability is low due to high surface albedo. This method of addressing measurement uncertainties in time series analysis is also applicable to other geophysical parameters. Trend estimates varied between −14 % and +5 % per decade and were significant (95.45 % confidence level) only for the month of October. Depending on the correction method, October trends varied between −11.4 % and −13.7 % for irradiance at 345 nm and between −11.7 % and −14.1 % for the UV Index. These large trends are consistent with trends in short-wave (0.3–3.0 µm) solar irradiance measured with pyranometers at NOAA's Barrow Observatory and can be explained by a change in snow cover over the observation period: analysis of pyranometer data indicates that the first day of fall when albedo becomes larger than 0.6 after snow fall, and remains above 0.6 for the rest of the winter, has advanced with a statistically significant trend of 13.6 ± 9.7 days per decade.

Correspondence to: G. Bernhard
(bernhard@biospherical.com)

1 Introduction

Solar ultraviolet (UV) radiation reaching the Earth's surface affects humans, terrestrial and aquatic ecosystems, and the chemical composition of the troposphere (UNEP, 2010; ACIA, 2005). UV radiation can cause sunburn, cataracts, and skin cancer in humans. Health benefits of UV radiation are principally derived from vitamin D production in the skin, which supports bone health and may decrease the risk of several internal cancers. Arctic inhabitants may experience high UV levels in the summer caused by reflections off of snow but the absence of UV radiation during winter months may result in Vitamin D deficiency (Holick, 2007). Changes in UV radiation (either up or down) can therefore affect health. UV effects on terrestrial ecosystems are often complex and indirect. For example, litter-decomposing fungi are sensitive to UV-B radiation (Gehrke et al., 1995; Moody et al., 1999) and this may affect the recycling of plant material. Plant exposure to UV-B radiation can change the composition of leaf tissue, which significantly affects the palatability and digestibility of food consumed by herbivores, including reindeer and caribou (Gwynn-Jones, 1999). Furthermore, changes in UV irradiance can reduce the productivity of marine ecosystems with effects on phytoplankton and species higher on the food chain (Hessen, 2001).

UV irradiance at the surface is affected by the solar elevation, stratospheric and tropospheric ozone concentrations,

Published by Copernicus Publications on behalf of the European Geosciences Union.

clouds, Rayleigh scattering on air molecules, surface albedo (e.g. snow cover, sea ice), aerosols, absorption by trace gases, and the Sun-Earth distance (WMO, 2007). Long-term changes in any of these parameters can lead to trends in UV radiation. For the Arctic, changes in ozone, albedo (snow and ice), and cloud cover are of particular importance.

Predictions of future ozone concentrations in the Arctic stratosphere have a large uncertainty because of their sensitivity to temperature. For example, heterogeneous reactions on the surfaces of polar stratospheric clouds (PSCs) are responsible for large losses in ozone observed in cold Arctic winters (WMO, 2011; Manney et al., 2011). There is a robust linear correlation between the ozone loss and the volume of vortex air with temperatures below −78 °C, the temperature threshold below which PSCs start to form (Rex et al., 2006). Because of the large uncertainty of current Chemistry-Climate Models to predict stratospheric temperatures (for example, many models tend not to capture the low temperatures observed in the Arctic lower stratosphere, WMO, 2011), there is in turn a large uncertainty in the evolution of Arctic spring-time ozone concentrations and surface UV intensities.

The extent of sea ice in the Arctic is currently decreasing rapidly due to climate change (Serreze et al., 2007). Models suggest that ice cover in summer will disappear within the next few decades (Comisco et al., 2008). Reduced surface albedo because of decreases in snow and ice cover will increase the fraction of solar energy absorbed by the Earth's surface. Organisms that were once living below snow and ice will be exposed to increased doses of UV, but organisms living above the surface will receive lower doses of UV due to the reduced reflectivity (UNEP, 2010). Climate models predict increased cloudiness and precipitation at high latitudes (Meehl et al., 2007), which would generally lead to decreases in UV radiation.

Surface UV irradiance can be derived from satellite measurements (e.g. Krotkov et al., 1998, 2001). These data sets have a large uncertainty for high latitudes because of the difficulty in distinguishing between snow and clouds from space (Tanskanen et al., 2007). When snow is misinterpreted as a cloud, the result is reduced below the value calculated for clear sky rather than increased. Particularly at coastal Arctic locations, ground-based measurements are more accurate than satellite observations, also implying that trend estimates are less prone to error.

In principle, trends in UV radiation can either be inferred from direct measurements (either from ground or space) or reconstructed based on proxy data such as total ozone and sun shine duration (e.g. Lindfors et al., 2003). Trends of summertime daily erythemal dose at 12 mid-latitude sites estimated with both methods for the period of 1980–2003 ranged between 2 % and 9 % per decade (WMO, 2011). Weatherhead et al. (1998) calculated that at least 15 yr of measurement are necessary to detect a trend of 5 % per decade in solar UV measurements with confidence. Considering that only very few UV data records are longer than 20 yr (e.g. Krzycin et al., 2011), the opportunity to derive meaningful trend estimates from direct measurements has arisen only recently.

The first attempt to estimate trends in solar UV irradiance at Barrow was presented by Gurney (1998). The data analysis was based on UV measurements of the years 1991 to 1995. According to this study, spectral irradiance at 305 nm increased by 3 to 10 % per year for all daylit months except June. These trends are much larger than those presented in this paper. It is likely that the large trends calculated by Gurney (1998) were partly a result of the abnormally small total ozone columns in 1992 and 1993, which were caused by high stratospheric aerosol concentrations following the eruption of Mt. Pinatubo in 1991 (WMO, 2003).

The UV radiation climate at Barrow and its influencing factors have been quantified by Bernhard et al. (2007). The authors also performed a preliminary trend analysis of UV-B, UV-A, and visible irradiance based on data of the years 1991–2005. Best estimates of trends varied between −23 % and +11 % per decade depending on data products and month but were generally not statistically significant. This paper extends this earlier analysis to the period 1991–2011.

Maintaining a 20+ yr data record at a low uncertainty level is a demanding task. Challenges include instrument failures, periods with degraded instrument performance, gaps in operational support, and drifts of calibration standards. All these factors affect trend estimates. Particular attention is given in the following analysis to the effect of measurement uncertainties on the detectability of trends. The method can also be applied to other environmental data sets.

The earlier analysis by Bernhard et al. (2007) showed that trend estimates for noontime and daily dose data are almost identical. Daily doses can only be accurately calculated when measurements throughout the day are available. This constraint reduces the number of days available for calculating a monthly average. The trend analysis presented in this paper is based on noontime measurements (22:00 UTC) because the number of noontime observations is generally larger than the number of days when a daily dose is available.

The earlier analysis also demonstrated that trends in UV radiation (and their sign) show large differences from month to month and that annualized trends are difficult to interpret. Trend estimates discussed in this paper are therefore based on monthly average data.

The uncertainty of a trend estimate depends on natural variability, the measurement uncertainty, and data gaps. All three sources of variability will be discussed in this paper. In general, it is not possible to unambiguously attribute an "outlier" in a measured time series to one of three mechanisms. For example, consider the following thought experiment involving three idealized experiments:

1. An ideal instrument with zero uncertainty is measuring temperature that is normally distributed about a constant value with a known standard deviation of x %.

2. A real instrument with a relative standard error of x % is measuring a constant temperature.

3. The real instrument of (2) measures the variable temperature of (1).

Experiments (1), (2), and (3) are repeated many times and a trend is estimated for every "run." For Experiments (1) and (2), the mean trend will be zero and the standard deviations (or uncertainties) calculated from the many individual trend estimates will be identical. Variability in measurements – caused either by real fluctuations in temperature (Experiment 1) or by uncertainties in the instrument (Experiment 2) – are therefore indistinguishable. For Experiment (3), the uncertainty of the trend estimate will be $\sqrt{2}$ times of that of Experiment (1) (or 2). In most circumstances, a priori knowledge of the instrument's measurement uncertainty does not allow to reduce the uncertainty of the trend estimate for the "real-world" Experiment (3). However, the trend uncertainty of Experiment (3) can be set in perspective to the hypothetical trend uncertainty of Experiment (2). For example, comparing the two uncertainties can help decide whether the uncertainty of the measurement apparatus may seriously affect the ability to detect statistically significant trends in temperature. Comparing the trend uncertainties derived from real-world measurements to that caused by measurement uncertainties will be an important part of this paper.

2 Data set

The trend analysis presented here is based on measurements of global (sun and sky) spectral irradiance performed between January 1991 and April 2011 with a high-resolution SUV-100 spectroradiometer. The instrument was historically part of the US National Science Foundation's UV Monitoring Network and is now a component of NSF's Arctic Observing Network. The instrument is installed into the roof of the Ukpeagvik Iñupiat Corporation building (71°19′29″ N, 156°40′45″ W, 8 m above sea level), which is located approximately 5.5 km northeast of the village of Barrow, Alaska, approximately 300 m inland from the Chukchi Sea, and 10 km away from Point Barrow, the northernmost point of Alaska. The land south and east of the system is flat tundra, which is snow-covered roughly between October and June (Stone et al., 2002). Annual cycles in sea ice and snow cover cause a large difference of surface albedo between summer and winter. General weather conditions and the radiation climate have been characterized by Maykut and Church (1973). Dutton et al. (2004) found that the annual average frequency of cloud occurrence has increased at Barrow from about 76 % of day time in 1976 to about 82 % in 2001. Over the same period, effective cloud transmission decreased significantly from 0.64 to 0.61. These trends in cloud characteristics led to a downward trend in annual average short-wave (0.3–3.0 µm) solar irradiance at the surface (Dutton et al., 2006).

The data set analyzed here has been referred to as "Version 2 data of the National Science Foundation's Ultraviolet Spectral Irradiance Monitoring Network". It has been described in detail by Bernhard et al. (2007). Measurements have been corrected for the instrument's cosine response error. Version 2 data are complemented with results of a radiative transfer model (Mayer and Kylling, 2005), which takes into account solar zenith angle, total ozone, vertical profiles of temperature and ozone, surface pressure, NO_2 absorption, and effective surface albedo. The model implementation has also been described by Bernhard et al. (2007).

Trends were estimated from two quantities retrieved from the Version 2 spectra: spectral irradiance integrated over the wavelength band of 342.5 to 347.5 nm (hereinafter called "irradiance at 345 nm" or E345), and the UV Index, which is a measure of the effectiveness of UV radiation to cause sunburn in human skin (WMO, 1998; WHO, 2002). The UV Index was calculated by weighting the measured spectra (provided in units of [µW cm^{-2} nm^{-1}]) with the action spectrum for erythema (McKinlay and Diffey, 1987) and multiplying the result by 0.4 cm^2 µW^{-1} (WHO, 2002). Trends were estimated on measurements performed at 22:00 UTC, which is the measurement closest in time to local solar noon at Barrow. Measurements at this time are available for the entire period. Monthly averages were calculated from the daily noontime measurements and trend estimates are based on these monthly means, denoted $\bar{E}(y_i, m)$, where y_i is year and m is month ($m = 1,\ 2, ...,\ 12$).

3 Trend analysis

A linear regression model was used to estimate monthly trends and their uncertainty. Using this model, the measured monthly mean irradiance $\bar{E}(y_i, m)$ can be written as:

$$\bar{E}(y_i, m) = a(m) + b(m)\, y_i + \varepsilon(y_i, m), \quad (1)$$

where $a(m)$ and $b(m)$ are the regression constant and slope, respectively, and $\varepsilon(y_i, m)$ are the residuals. For simplicity, the argument m is omitted in the following. The values of the parameters a and b were calculated by minimizing the merit function $\sum_{i=1}^{n} \left(\bar{E}(y_i) - a - b y_i\right)^2$, where n is the number of years considered. The residuals $\varepsilon(y_i)$ can be written as:

$$\varepsilon(y_i) = \varepsilon_S(y_i) + \varepsilon_U(y_i) + \varepsilon_G(y_i), \quad (2)$$

where $\varepsilon_S(y_i)$ is the component resulting from natural causes such as year-to-year variations in the atmospheric transmission. $\varepsilon_U(y_i)$ is resulting from the measurement uncertainty, expressed as a "standard uncertainty" (ISO, 1993) and denoted $u_U(\bar{E}(y_i))$. $\varepsilon_G(y_i)$ results from the uncertainty in the

calculation of a monthly average if there are gaps in the data series.

The uncertainty of trend estimates is determined by the variance of the measured values $\bar{E}(y_i)$ and can generally not be reduced by knowing $u_U(\bar{E}(y_i))$. For example, let us assume that there is an exact linear relationship between the year and the actual monthly mean irradiance (that is, $\varepsilon_S(y_i) = 0$ for all y_i). The values of the two coefficients a and b are determined by linear regression from the measurements $\bar{E}(y_i)$, which are affected by the uncertainty $u_U(\bar{E}(y_i))$. For this hypothetical case, the uncertainties of the estimated values for a and b do generally not depend on whether or not the uncertainty $u_U(\bar{E}(y_i))$ is known a priori. Exceptions from this rule may apply under certain circumstances. For example, Hicke et al. (2008) used a parametric bootstrap technique and knowledge of $u_U(\bar{E}(y_i))$ to obtain a confidence interval for b. A more conservative approach is used here: I calculate the uncertainty of b (denoted $u(b)$), from the variability of the measured data; use $u_U(\bar{E}(y_i))$ to calculate a theoretical uncertainty of b (denoted $u_U(b)$), which results from the hypothetical case that $\varepsilon_S(y_i)$ and $\varepsilon_G(y_i)$ are zero for all y_i; and finally compare $u_U(b)$ with $u(b)$.

Before a regression is attempted, it is imperative to remove known systematic errors from the daily irradiances that are used to calculate the monthly mean irradiances and systematic errors caused by data gaps. The determination of these errors is also subject to uncertainty. Different methods to correct systematic errors in the measurements have been explored and are discussed in Sect. 3.1. The uncertainty $u_U(\bar{E}(y_i))$ is quantified in Sect. 3.2. The correction for data gaps and the standard uncertainty of this correction, denoted $u_G(\bar{E}(y_i))$, are described in Sect. 3.3. The different correction schemes result in several different data sets for $\bar{E}(y_i)$. Regressions were performed on all data sets to test the sensitivity of the derived trends on the choice of the correction method.

Data of all months were tested for autocorrelation using the Durbin-Watson Test (Draper and Smith, 1998). No autocorrelation was found between measurements of consecutive years. "d"-values of the Durbin-Watson statistics for the different months range between 1.34 and 2.50. The median is 2.0, i.e. the ideal value for a data set that is not autocorrelated. Autocorrelation was therefore not considered when calculating the uncertainties of regression slopes.

The uncertainty of the regression slope $u(b)$ is calculated based on the propagation-of-error principle for uncorrelated variables (e.g. Press et al., 1986):

$$u(b) = \left[\sum_{i=1}^{n} \left[u(\bar{E}(y_i)) \right]^2 \left(\frac{\partial b}{\partial \bar{E}(y_i)} \right)^2 \right]^{0.5}. \quad (3)$$

The partial derivative $\partial b \big/ \partial \bar{E}(y_i)$ expresses the sensitivity of the regression slope b to a change in the measured value $\bar{E}(y_i)$. The uncertainty $u(\bar{E}(y_i))$ is assumed to be independent of i and calculated as the sample standard deviation of the residuals for two degrees of freedom:

$$u(\bar{E}(y_i)) \equiv u(\bar{E}) = \sqrt{(n-2)^{-1} \sum_{i=1}^{n} [\varepsilon(y_i)]^2}. \quad (4)$$

To calculate the hypothetical uncertainty $u_U(b)$ of a regression slope resulting from measurement uncertainties, the term $u(\bar{E}(y_i))$ in Eq. (3) has to be replaced by $u_U(\bar{E}(y_i))$:

$$u_U(b) = \left[\sum_{i=1}^{n} \left[u_U(\bar{E}(y_i)) \right]^2 \left(\frac{\partial b}{\partial \bar{E}(y_i)} \right)^2 \right]^{0.5}. \quad (5)$$

Similarly, the standard uncertainty of $\bar{E}(y_i)$ related to data gaps is denoted $u_G(\bar{E}(y_i))$, and the hypothetical uncertainty of the regression slope resulting from $u_G(\bar{E}(y_i))$ is denoted $u_G(b)$. To calculate $u_G(b)$, the term $u(\bar{E}(y_i))$ in Eq. (3) has to be replaced by $u_G(\bar{E}(y_i))$:

$$u_G(b) = \left[\sum_{i=1}^{n} \left[u_G(\bar{E}(y_i)) \right]^2 \left(\frac{\partial b}{\partial \bar{E}(y_i)} \right)^2 \right]^{0.5}. \quad (6)$$

Trends are calculated at a confidence level of 95.45 %. (I chose a level of 95.45 % rather than the level of 95.0 % that is often used because 95.45 % is the percentage of values within $\pm 2\sigma$ of a normal distribution.)

Percentual decadal trends T were calculated relative to the year 2000: $T[\%] = 1000 \times b/(a + 2000 \times b)$. The uncertainty of the trend, denoted $u(T)$, is $u(T)[\%] = 1000 \times u(b) \times t(n-2, 0.9545/2)/(a + 2000 \times b)$, where $t(n-2, 0.9545/2)$ is the value of Student's t-distribution for n samples and a confidence level of 95.45 %. Trend uncertainties associated with the uncertainties $u_U(b)$ and $u_G(b)$ were calculated similarly and are denoted $u_U(T)$ and $u_G(T)$.

Using Student's t-test for determining the significance of trends is only appropriate if residuals $\varepsilon(y_i)$ are normally distributed. Normality was tested with the Anderson-Darling test (Stephens, 1974). The test's A^2-statistic was smaller than 0.7 for all months, both for E345 and UV Index data. This suggests that the null-hypothesis that data are normally distributed cannot be rejected ($p < 0.05$). The t-test is therefore suitable.

The propagation-of-error principle suggests that

$$(u(T))^2 = (u_S(T))^2 + (u_U(T))^2 + (u_G(T))^2, \quad (7)$$

where $u_S(T)$ is the uncertainty in the trend estimate resulting from natural variability alone. This quantity indicates the uncertainty of the trend that could be expected from measurements of an ideal instrument. Real trends must be outside the range of $T \pm u_S(T)$ such that they can be detected with an ideal instrument with confidence. The uncertainty of $u_S(T)$ is therefore a principle limit for trend detection given by natural variability.

The ratios of $R_U(T) \equiv (u_U(T))^2 \big/ (u(T))^2$ and $R_G(T) \equiv (u_G(T))^2 \big/ (u(T))^2$ were also calculated to judge the contribution of the measurement and gap variances to the overall trend variance $(u(T))^2$.

3.1 Detection and correction of systematic errors

Comparing measured UV spectra with spectra calculated with a radiative transfer model is a useful method to assess the quality of the measurements and to detect significant errors in measurements that may change over time (Bernhard et al., 2004, 2008). The method is most accurate for periods when the state of the atmosphere and the surface albedo are well defined. At Barrow, these conditions are usually met during clear-sky periods in the summer when aerosol concentrations are small and the surface is free of snow. For example, the surface albedo of tundra during the snow-free months of June through September can be assumed to be constant at about 5 % in the UV (Blumthaler and Ambach, 1988). Assuming that there are no trends in unknown atmospheric absorbers, the ratio of the measured and modeled spectral irradiance during cloud-free period in the summer should be similar for every year, and variations of this ratio over time may indicate a drift in the measurements. (There may still be a systematic bias between measurement and model due to invariant systematic errors in either the measurements or the calculations. However, such a bias would not affect long-term trend estimates.)

Model spectra that are part of the Version 2 data set use effective surface albedo (Lenoble et al., 2004) and total ozone column as input parameters. Both parameters are calculated from the measurements (Bernhard et al., 2004). Version 2 data are therefore not independent from model results. The ratio of measurement and model is therefore a less-useful quality control tool for months when the ground is covered by snow or at wavelengths that are affected by ozone absorption. Fortunately many systematic errors, such as the drift in the output of calibration lamps, have only a modest wavelength dependence. Temporal variations in the ratio of measurement and model at 345 nm, where ozone absorption is negligible, are therefore also good indicators for instrument drifts below 340 nm where ozone absorption is important.

The analysis is based on spectra measured at solar zenith angles (SZA) smaller than 80°. The limitation has two reasons. First, measurements and model calculations are more challenging at large SZAs and the value of using model calculations as a quality control tool is reduced at large SZAs. Second, trend estimates presented in this paper are based on noontime measurements when the SZA is smaller than 80° (with the exception of data measured before 26-February or after 15-October when SZA is larger than 80°). Some Version 2 spectra are flagged for inferior quality. These measurements were also excluded from the data analysis.

In theory, the consistency of measurements over time could also be tested by comparing clear-sky irradiances measured at the same SZA during different years. In practice, this method is problematic as clear-sky conditions occur in different periods every year.

The method of using model spectra to quality-control measurements is similar to that presented by Bernhard et al. (2007). Only a summary of the implementation is provided here. First, clear-sky periods are determined based on temporal variability using the method by Bernhard et al. (2008). Spectra measured under stable overcast conditions that passed this criterion were identified and removed. Second, spectra measured during these periods for $\mathrm{SZA} < 80°$ are ratioed to the associated "clear-sky" model spectra of the Version 2 data set. In the third step of the analysis, the medians of these "ratio spectra" are calculated on a wavelength-by-wavelength basis from all ratio spectra within preset sample intervals. These sample intervals include entire years (e.g. 1991, 1992, ..., 2011), months (e.g. January 1991, February 1991, ..., April 2011), and low-albedo summer periods (e.g. 1 July–30 September 1991, 1 July–30 September 1992, ..., 1 July–30 September 2010). Lastly, these "median-ratio-spectra" are averaged over the wavelength range 340–350 nm. The resulting "q-ratios" are denoted $q_{\mathrm{annual}}(y)$, $q_{\mathrm{monthly}}(y,m)$, and $q_{\mathrm{summer}}(y)$, respectively, where y is year ($y = 1991, 1992, ..., 2011$) and m is month ($m = 1, 2, ..., 12$). The three quantities are shown in Fig. 1. The q-ratios vary between 0.79 and 1.08 with the majority of values being between 0.94 and 1.02. The medians of the q-ratios are 0.970, 0.973, and 0.963, respectively, and are denoted $\bar{q}_{\mathrm{annual}}$, $\bar{q}_{\mathrm{monthly}}$, and $\bar{q}_{\mathrm{summer}}$.

The expanded uncertainty of measurements of Version 2 UV data is 6.0 % (Sect. 3.2). To contrast this value with the variation of the q-ratios, Fig. 1 also includes lines at 1 ± 0.060 (yellow lines) and $\bar{q}_{\mathrm{monthly}} \pm 0.060$ (orange lines). Most q-ratios fall within the two limits but some are outside. The possible reasons leading to these outliers are discussed in Appendix A.

$q_{\mathrm{summer}}(y)$ tends to be larger between 1992 and 2001 compared to 2002–2010. This step change may be explained by the modification of the instrument's cosine collector at the beginning of 2001 (Bernhard et al., 2007). The differences in the angular response of the old and new collector were address by the cosine-error correction, but may not have been removed completely. Results presented in Sect. 4 indicate that the step change has a noticeable effect on trend estimates.

Data were corrected by scaling measurements using the results of the measurement-to-model comparison. For example, in order to utilize the $q_{\mathrm{annual}}(y)$ values for the correction, all measurements performed in year y were multiplied with the correction factor $C_{\mathrm{annual}}(y) \equiv \bar{q}_{\mathrm{annual}}/q_{\mathrm{annual}}(y)$. Likewise, the values of $q_{\mathrm{summer}}(y)$ and $q_{\mathrm{monthly}}(y,m)$ were used by multiplying the noontime measurements with $C_{\mathrm{summer}}(y) \equiv \bar{q}_{\mathrm{summer}}/q_{\mathrm{summer}}(y)$ and $C_{\mathrm{monthly}}(y,m) \equiv \bar{q}_{\mathrm{monthly}}/q_{\mathrm{monthly}}(y,m)$, respectively. If q-ratios for a certain month were not available (for example because the number of clear-sky days was not sufficient), the correction factor was set to 1. For reasons explained above, $C_{\mathrm{summer}}(y)$ should be the most accurate correction factor, however, the factor may not be the most appropriate for years when the systematic errors changed between spring and summer.

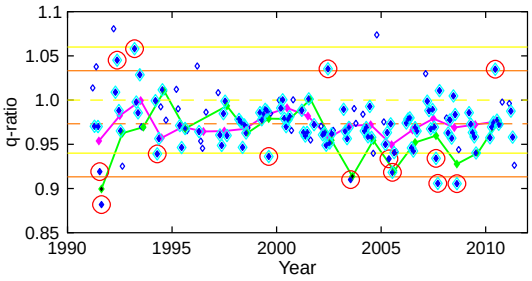

Fig. 1. Ratios between measurement and model at 345 nm for different averaging intervals ("q-ratios"). Open blue symbols: monthly q-ratios ($q_{\mathrm{monthly}}(y,m)$); solid blue symbols: subset of $q_{\mathrm{monthly}}(y,m)$ where the median was calculated from at least 10 spectra; pink solid symbol connected by lines: $q_{\mathrm{annual}}(y)$; green solid symbol connected by lines: $q_{\mathrm{summer}}(y)$. Outliers are indicated by red circles and discussed in Appendix A. $q_{\mathrm{monthly}}(y,m)$ used for the correction are indicated by a cyan border. Values of $q_{\mathrm{summer}}(y)$ not used for the correction have a black core. Broken lines drawn in yellow (orange) indicate 1.0 ($\bar{q}_{\mathrm{monthly}}$). Solid lines drawn in yellow (orange) indicate the range of 1 ± 0.060 ($\bar{q}_{\mathrm{monthly}}\pm0.060$).

3.2 Measurement uncertainty

The uncertainty of spectra measured with the SUV-100 spectroradiometer at Barrow has been discussed by Bernhard et al. (2007). For a SZA of 45°, the expanded relative uncertainty (coverage factor $k=2$, equal to a confidence interval of 95.45 %) of erythemal irradiance varies between 5.8 % and 6.2 % and depends only little on year. The corresponding range for SZA = 80° is 5.8–8.8 %. Uncertainties are dominated by "type B" uncertainties (ISO, 1993), which do not change with averaging. Based on these considerations, the relative standard uncertainty $u_U(\bar{E}_i)/\bar{E}_i$ of the monthly means was set to 3 % for all years and months.

3.3 Correction for gaps in data set

The monthly mean irradiances $\bar{E}_i$ were calculated by averaging all available noontime measurements of a given month. If a measurement of a single day was missing, but measurements of the previous and subsequent days were available, the value for the missing day was calculated as average of the measurements of the two adjacent days. No uncertainty was attributed to this procedure. Months with more than 10 missing days were not used for the trend analysis (Table 1). There will be a bias in the monthly average if periods with missing days are not equally distributed. For example, solar radiation tends to increase during months in the spring because the noontime SZA decreases. If measurements are missing at the beginning of a month, the monthly average will be biased high. To correct for this effect, for every day of the year, the average was calculated from measurements of all years, resulting in a climatological "mean cycle" of UV radiation at Barrow. In a second step, two averages were calculated from this mean cycle, one that uses all values of a given month, denoted $A(m)$, and one (denoted $A^*(y,m)$) that is based only on those days of this mean cycle that are available in the data set for year y and month m that needs adjustment. Monthly averages are corrected by multiplication with the "gap correction factor" $C_G(y,m)\equiv A(m)/A^*(y,m)$. For example, suppose the monthly mean of March 2001 is to be corrected. In this month, measurements of the first five days are missing. First, the average of all available noontime measurements of this month is calculated, resulting in the "uncorrected monthly average" for March 2001, denoted $\bar{E}_u(2001,3)$. Second, the mean cycle is averaged over March (days 60 to 90), resulting in $A(3)$. Third, the mean cycle is averaged over days 65 to 90 (i.e. the first five days of March are omitted), resulting in $A^*(2001,3)$. Lastly, the "corrected monthly average" for March 2001 ($\bar{E}_c(2001,3)$), is determined:

$$\begin{aligned}\bar{E}_c(2001,3) &= \bar{E}_u(2001,3)\frac{A(3)}{A^*(2001,3)}\\ &= \bar{E}_u(2001,3)C_G(2001,3).\end{aligned} \quad (8)$$

The correction mostly takes into account climatological variations in SZA and ozone (e.g. the mean Dobson-Brewer circulation), which repeat every year. Variations in total ozone occurring during the periods of data gaps are not taken into account. The relative standard uncertainty associated with this correction, $u_{G,\mathrm{rel}}(y,m)$, is calculated as

$$u_{G,\mathrm{rel}}(y,m)=\frac{1}{\sqrt{3}}|C_G(y,m)-1|. \quad (9)$$

The calculation of $u_G(y,m)$ is based on the assumption that the probability distribution function of $\bar{E}_c(y,m)$ is rectangular; that is, the probability that the true value of the monthly average, $\bar{E}_t(y,m)$, lies within the interval $[\bar{E}_c(y,m)/C_G(y,m),\ \bar{E}_c(y,m)\times C_G(y,m)]$ is constant and is zero outside this interval (ISO, 1993). This is a conservative estimate of the uncertainty.

4 Results

Trends in monthly mean noontime UV radiation $\bar{E}(y_i)$ were determined for E345 and the UV Index. Four different data sets were considered for each quantity based on different corrections for systematic errors. These are: no correction (Method 1); and corrections using the correction factors C_{annual} (Method 2), C_{summer} (Method 3), and C_{monthly} (Method 4). The "gap correction" (Sect. 3.3) was applied to all data sets.

Figure 2 shows the result of the time series analysis for the monthly mean noontime irradiance at 345 nm. Data have been corrected with Method 4. The figure is divided into nine panels for the months of February through October. Each panel indicates the monthly means $\bar{E}(y_i)$, the measurement uncertainty $u_U(\bar{E}(y_i))$, the trend estimate T (expressed in

Table 1. Number of days used for the calculation of the monthly average. Months with more than 10 missing days were not used in the trend analysis and are shown in parentheses.

Year	Feb	Mar	Apr	May	Jun	Jul	Aug	Sep	Oct
1991	26	27	30	26	(19)	30	31	30	31
1992	29	31	30	27	30	29	29	30	31
1993	21	31	30	31	30	31	31	30	31
1994	(14)	31	28	31	25	27	27	26	24
1995	18	30	30	27	30	21	31	28	22
1996	29	27	25	26	22	26	31	30	31
1997	28	31	30	31	30	31	31	30	25
1998	28	31	30	(17)	25	31	21	30	31
1999	28	31	30	31	30	31	31	30	31
2000	29	31	30	27	30	31	31	30	31
2001	18	31	30	27	30	31	31	30	25
2002	28	31	30	31	30	31	31	30	31
2003	28	31	30	31	30	23	31	30	31
2004	29	24	30	28	30	31	23	(8)	31
2005	25	(20)	26	(12)	24	31	31	28	31
2006	28	(15)	(15)	29	30	31	31	23	31
2007	25	27	30	31	30	25	22	(18)	31
2008	26	31	30	25	30	31	29	30	31
2009	28	29	30	31	28	(12)	(0)	(0)	(0)
2010	(0)	(12)	(10)	(20)	(8)	31	31	30	31
2011	22	26	30	(1)	(0)	(0)	(0)	(0)	(0)

percent per decade), the uncertainty of the trend $u(T)$, the correlation coefficient (R^2), the uncertainty of the trend that can be explained with the measurement uncertainty $u_U(T)$, and the trend uncertainty caused by gaps $u_G(T)$. The hyperbolic confidence bands associated with each of the three uncertainties are also indicated and were calculated according to Draper and Smith (1998).

The following can be concluded from the results presented in Fig. 2:

- Trend estimates range between −14 % (October) and +3 % (May) per decade.
- The trend uncertainty ranges between 3 % (February and April) and 13 % (September). The uncertainty is much smaller in the spring than in the fall. This can be explained with the smaller natural variability in the spring when the albedo is large and variability due to cloud attenuation is greatly reduced (Ricchiazzi et al., 1995; Nichol et al., 2003).
- Trends are not significant at the 95.45 % confidence level for any month, except for October, where the trend is -14 ± 12 % per decade.
- $u_U(T)$ is 3 % for all months. Because of the small natural variability in spring, $u_U(T)$ has a much larger effect on the detectability of trends during the first part of the year compared to fall, when the natural variability outweighs the effect of the measurement uncertainty.
- $u_G(T)$ ranges between 0 % and 3 %, and is an important factor for the detectability of trends only for the month of February.

Trend calculations were repeated using the data sets corrected with Methods 1, 2 and 3, to quantify the sensitivity of the trend estimates on the treatment of systematic errors. Results of the trend estimates T and the associated uncertainty $u(T)$ are shown in Fig. 3. Results of Methods 1, 2, and 4 are generally very similar, but trends determined by Method 3 are 1.7 % larger on average. This is caused by the step-change of $C_{\text{summer}}(y)$, with lower values for the years 1992–2001 than for the 2002–2010 period.

Figure 4 is similar to Fig. 2, but shows the result of the time series analysis for the UV Index. The following can be concluded from the results presented in Fig. 4:

- Trend estimates range between −14 % (October) and +5 % (August) per decade.
- The trend uncertainty ranges between 4 % (February) and 13 % (September), is smaller in the spring than in the fall, but tends to be larger than the trend uncertainty calculated for irradiance at 345 nm.
- Only the trend for October is significant; it is -14 ± 13 % per decade.

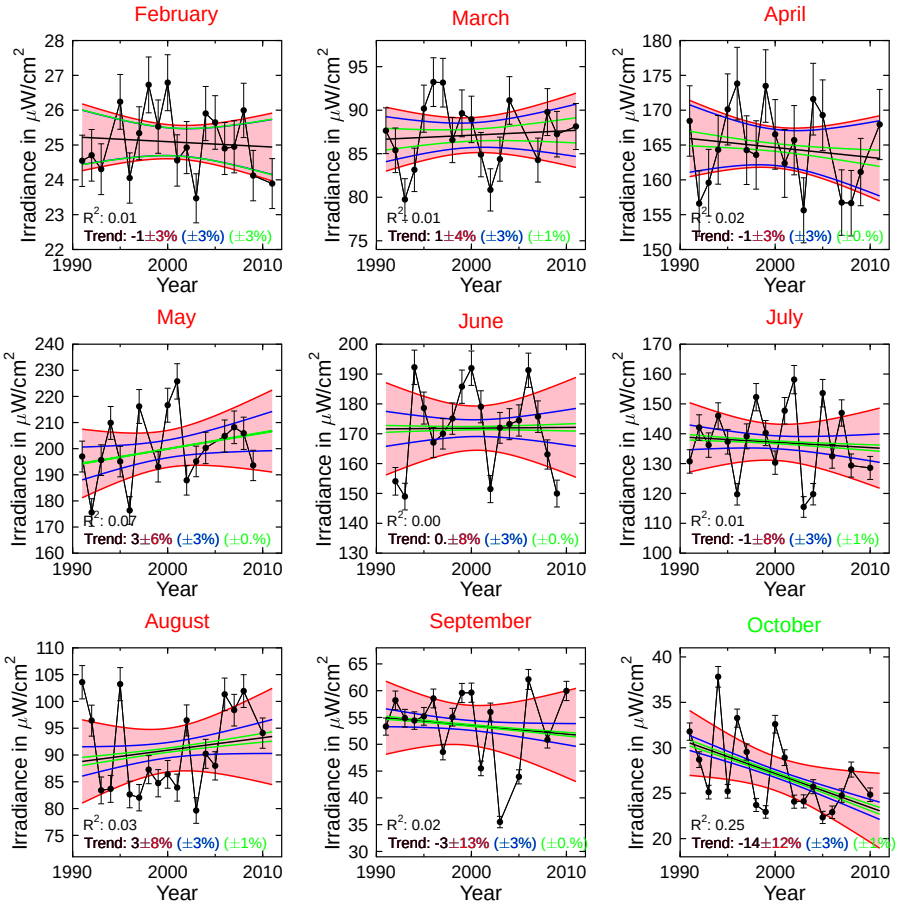

Fig. 2. Time series analysis of irradiance at 345 nm. Each panel shows results for a different month, starting with February (top left) and ending with October (bottom right). Black symbols connected by black lines indicate the monthly means $\bar{E}(y_i)$ of measured noontime spectral irradiance at 345 nm. Data have been corrected for systematic error using Method 4. Error bars indicate the measurement uncertainty $u_U(\bar{E}(y_i))$. Trend estimates are indicated by black lines. Their 95.45 % confidence bands are shown in pink shading. The lower half of each plot gives the square of the correlation coefficient (R^2), the estimate of the decadal trend T (black number), the uncertainty of the trend estimate $u(T)$ (red number), the uncertainty of the trend that can be explained with the measurement uncertainty $u_U(T)$ (blue number), and the trend uncertainty caused by gaps $u_G(T)$ (green number). The hypothetical confidence bands associated with the measurement uncertainty and the gap uncertainty are indicated by blue and green lines, respectively.

– $u_U(T)$ is 3 % for all months. $u_G(T)$ ranges between 0 % and 4 %, and is an important factor for the detectability of trends only for the month of February.

Trend calculations were again repeated using the data sets corrected with Methods 1, 2 and 3. The difference between maximum and minimum trend estimate for each month varies between 1.5 % (February) and 2.9 % (June). Trends estimated with Method 3 are 1.7 % larger on average. The difference between the maximum and minimum uncertainty of the trend estimates varies between 0.2 % (September) and 1.1 % (April and June). These results are very similar to those obtained for the trend in irradiance at 345 nm.

Table 2 provides a compilation of all relevant parameters of the trend analysis. Monthly trends were generally calculated based on data of 17 to 19 yr. $u_U(T)$ ranges between 2.5 % and 3.0 %. $u_G(T)$ exceeds 3 % in February and varies between 0.1 and 1.5 % for the other months. For irradiance at 345 nm, the ratio of the variance caused by the measurement uncertainty to the observed variance, $R_U(T)$, is larger than 50 % in February, March, and April; varies between 20 % and 33 % in May (depending on the correction method); is between 10 % and 20 % for May–August; and below 10 % in September and October. For the UV Index, ratios of $R_U(T)$ are generally smaller than those calculated for irradiance at 345 nm because monthly variations of the UV Index are also influenced by ozone variations. The contribution of $u_U(T)$ to the overall variability is therefore smaller. The ratio of the variance caused by gaps to the observed variance, $R_G(T)$, exceeds 60 % in February and is below 10 % for the other months, indicating again that the contribution of gaps in the

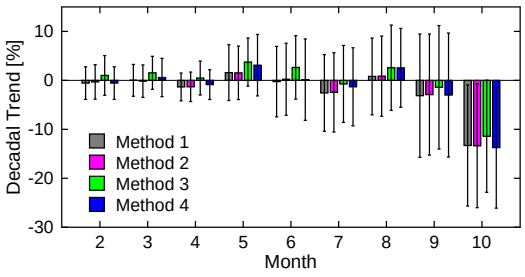

Fig. 3. Comparison of trends and their uncertainties of irradiance at 345 nm obtained for the four data sets discussed in the text. Method 1 is based on the uncorrected dataset. Methods 2–4 apply correction factors based on ratios of clear sky measurements and model calculations that were averaged over annual (Method 2), summerly (Method 3) and monthly (Method 4) periods.

time series is unimportant for trend detection. For February, the sum of $(u_U(T))^2$ and $(u_G(T))^2$ is larger than $(u(T))^2$. $(u_S(T))^2$, calculated with Eq. (7), becomes therefore negative, which is an impossible result. The uncertainty attributed to data gaps is likely too large for February because of its conservative estimate with Eq. (9). For all months but February, the difference between $u(T)$ and $u_S(T)$ varies between 0.3 % (October) and 1.4 % (April), suggesting again that reducing the measurement uncertainty would be mostly beneficial for measurements in the spring, but would have little effect on the ability to detect trends for low-albedo months.

5 Discussion

The most striking result of the trend analysis is the large and statistically significant downward trend in UV irradiance of about 14 % per decade for October. I hypothesize that this trend is caused by changes in snow cover and the resulting changes in surface albedo.

Surface albedo increases downwelling irradiance because a fraction of photons reflected upward by the surface are scattered downward by air molecules (clear sky case) and cloud droplets. Model calculations for a SZA of 80° (noontime SZA at Barrow on 15 October) indicate that an increase in albedo from 5 % to 80 % (a typical value for Barrow during winter, Bernhard et al., 2007) will increase spectral irradiance at 345 nm by 38 % for clear skies and by a factor of 2.97 for overcast skies (cloud optical depth of 50). For clear skies, high surface albedo has a larger effect on UV than visible irradiance due to the wavelength dependence of Rayleigh scattering. However, this wavelength-dependence is largely reduced for overcast situations. According to my model calculations, a change in albedo from 5 % to 80 % during overcast conditions will increase global spectral irradiance at 600 nm by a factor of 2.89, which is only slightly below the factor of 2.97 calculated for 345 nm.

To determine whether changes in snow cover have occurred during the last 20 yr, measurements of upwelling and downwelling short-wave irradiance measured by pyranometers at the Barrow Observatory of NOAA's Global Monitoring Division (GMD) were analyzed. The facility is located 2 km east of the UV spectroradiometer. Data are part of the Baseline Surface Radiation Network (BSRN) and are available for the years 1992–2009. Albedo was calculated by dividing upwelling with downwelling irradiance. Snow cover usually leads to a distinct change in albedo from below 0.2 (no snow) to above 0.7 (snow). I determined the first day of fall when albedo becomes larger than 0.6 and remains above 0.6 for the rest of the winter. Results shown in Fig. 5 indicate that this day has advanced considerably during the last 20 yr with a statistically significant trend of 13.6 ± 9.7 days per decade (blue dataset in Fig 5). A similar analysis using an albedo value of 0.4 as threshold resulted in an almost identical trend of 12.7 ± 8.6 days per decade. Note that the date of persistent snow cover was not well defined in 2006 because of a melting period in mid-October; the data point for 2006 is therefore missing. For the period 1995–2008, the day of the start of persistent snow cover anti-correlates well with the monthly mean irradiance at 345 nm for October (red dataset in Fig. 6). The coefficient of determination R^2 is 0.73. As the day of permanent snow-cover is getting progressively later, the fraction of the month with high surface albedo is decreasing. Reduced surface albedo leads to less UV radiation. The good anti-correlation between the start of persistent snow cover and E345 suggests that the dominant fraction of the trend in E345 is caused by changes in snow cover. There is no good correlation for the years 1991–1994. This may have several reasons. First, the period 1991–1993 was affected by aerosols from the Mt. Pinatubo eruption, which has lowered the surface irradiance by a few percent (e.g. Bernhard et al., 2007). Second, during this period, the day of the start of persistent snow cover already occurred in September and a good correlation with E345 for October cannot be expected. Third, factors other than albedo such as cloud cover contribute to the variability.

The trend of downwelling short-wave irradiance at Barrow was also estimated. For these calculations, a new and revised pyranometer dataset provided by Ellsworth G. Dutton of NOAA GMD was used. This dataset is more accurate than that previously available from BSRN for Barrow, although, the data at BSRN are being revised and will match the data used here. For October, the trend of the monthly mean noontime irradiance calculated for the period 1991–2010 was -8.3 ± 10.9 % per decade. This trend estimate is somewhat smaller than the trend calculated for E345. The smaller trend is consistent with the wavelength dependence of the albedo effect discussed earlier. The October trend for irradiance in the visible (400–600 nm) calculated from the Version 2 spectra of the SUV-100 is -14.4 ± 16.6 %.

The day of the year when albedo drops below 0.3 at the end of winter was also calculated. The time of snow melt varied between day 145 (25 May) and 167 (16 June). A similar analysis has been conducted by Stone et al. (2002) for the

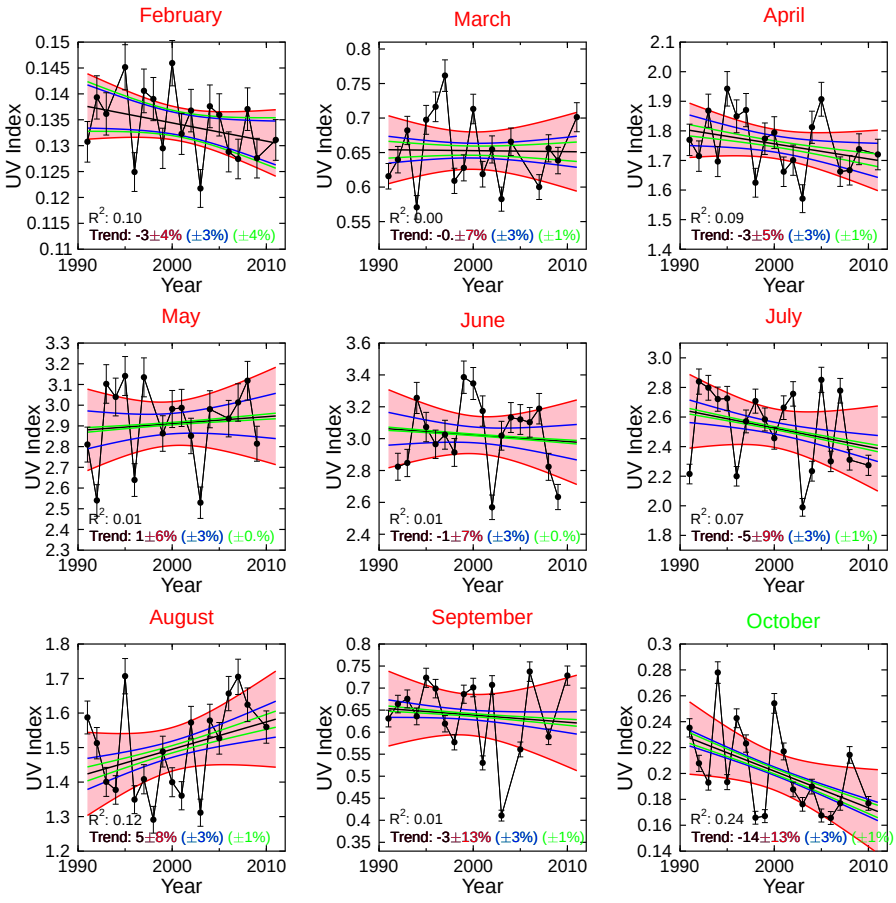

Fig. 4. Same as Fig. 2, but for the UV Index.

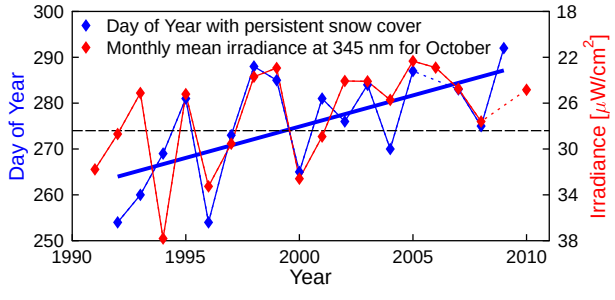

Fig. 5. Comparison of onset of snow cover and irradiance at Barrow. Blue symbols, left axis: day of year when surface albedo becomes larger than 0.6 and stays above 0.6 for the rest of the winter. Heavy blue line: linear regression to this dataset. The date of persistent snow cover was not well defined in 2006, and the associated data point is missing (broken blue line). Red symbols, right axis: monthly mean irradiance at 345 nm for October. Note that the right axis is reversed. No data are available for 2009 (broken red line). The broken black line indicates 1 October.

period 1941–2000. An update of the analysis spanning the years 1941–2009 is available at http://www.esrl.noaa.gov/gmd/grad/snomelt.html. Snow melt now occurs 10 days earlier than at the beginning of this 68-yr period. Most of the advance has occurred since the mid 1970s and is coinciding with a major shift in atmospheric circulation that occurred in the North Pacific beginning in 1976 (Stone et al., 2005). The trend estimate for the period 1992–2009 is -1.4 ± 5.9 days per decade. This trend is an order of magnitude smaller than that calculated for the onset of snow cover in the fall discussed above, and not statistically significant. The absence of a trend in UV irradiance for June (Table 2) is consistent with the lack of a clear change in the timing of snow melt over the last two decades.

It is of interest to compare trend estimates for the UV Index with trends in total ozone. Total ozone was retrieved consistently for all years from measured UV spectra according to Bernhard et al. (2003). The algorithm takes seasonal variation in the vertical ozone and temperature profiles into account and has been validated against measurements of a Dobson photometer operated by NOAA at Barrow and observations from the Total Ozone Mapping Spectrometer (TOMS)

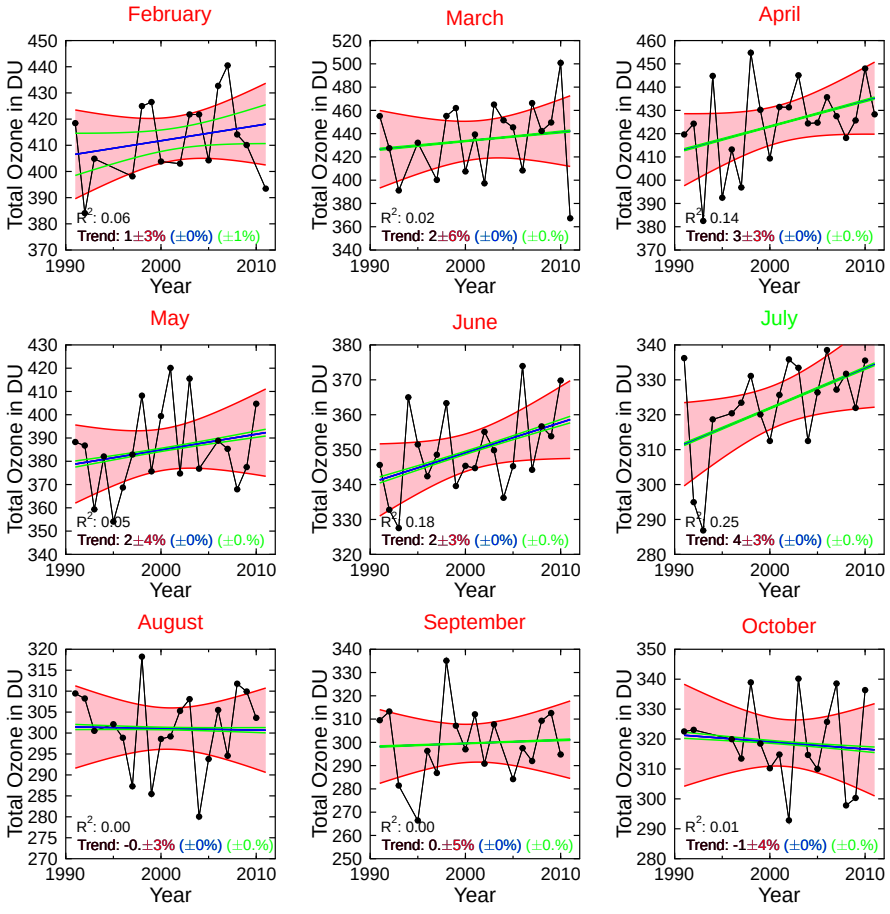

Fig. 6. Same as Fig. 2, but for total ozone. The measurement uncertainty was set to zero.

on NASA's Earth Probe satellite (Bernhard et al., 2003). Ozone data are not available for every day where UV data are available. The maximum number of missing days per month allowed for calculating monthly average ozone columns had to be relaxed from 10 days used for UV trends to 20 days. The same "gap correction" method as applied to UV data was used. Uncertainties in decadal ozone trends caused by gaps were smaller than 0.4 % for all months, with the exception of February where the uncertainty was 1.4 % (Table 2). Figure 6 shows trend estimates of total ozone. Trends are not statistically significant with the exception for the trend for July, which is 3.6 ± 3.3 % (Table 2).

The relationship between the percental change in the UV Index and the associated percental changes in total ozone is often expressed with Radiation Amplification Factors (RAF) (Booth and Madronich, 1994). For SZAs between 0° and 50°, RAF is about 1.1, meaning that a 1 % decrease in total ozone causes a 1.1 % increase in the UV Index. RAF depends somewhat on solar zenith angle and total ozone and is often smaller than 1 for the large SZAs prevailing at high latitudes (Micheletti et al., 2007; WMO, 2011). Trends in the UV Index, denoted $\hat{T}_{\mathrm{UVI}}(m)$, were estimated from trends in total ozone ($T_{\mathrm{O_3}}(m)$) and trends in E345 ($T_{\mathrm{E345}}(m)$) using the relationship

$$\hat{T}_{\mathrm{UVI}}(m) = T_{\mathrm{E345}}(m) - \mathrm{RAF}(\overline{\mathrm{SZA}}(m), \overline{\mathrm{O_3}}(m)) \times T_{\mathrm{O_3}}(m), \quad (10)$$

where $\overline{\mathrm{SZA}}(m)$ and $\overline{\mathrm{O_3}}(m)$ are the average noontime SZA and average total ozone column for month m, respectively. $\mathrm{RAF}(\overline{\mathrm{SZA}}(m), \overline{\mathrm{O_3}}(m))$ is the associated Radiation Amplification Factor. Equation (10) assumes that trends in the UV Index caused by factors other than ozone (e.g. clouds and albedo) can be characterized with $T_{\mathrm{E345}}(m)$. In Table 3, the estimated trend of the UV Index, $\hat{T}_{\mathrm{UVI}}(m)$, is compared with UV Index trends determined from the regression analysis of Sect. 4, $T_{\mathrm{UVI}}(m)$. The difference between $T_{\mathrm{UVI}}(m)$ and $\hat{T}_{\mathrm{UVI}}(m)$ is smaller than ± 1.3 %, except for August when the difference is 2.6 %. These differences are well within the uncertainty of the trend analysis and confirm that the trends of $T_{\mathrm{E345}}(m)$, $T_{\mathrm{UVI}}(m)$, $T_{\mathrm{O_3}}(m)$ are self-consistent. Trends in the UV Index controlled for trends in E345 (i.e. $T_{\mathrm{UVI}}(m) - T_{\mathrm{E345}}(m)$) anti-correlate with trends in ozone $\overline{\mathrm{O_3}}(m)$ for the months of February through August, as would be expected. UV Indices in September and October do not anti-correlate with trends in ozone, which may be

Table 2. Statistics for trend analysis. Irradiance at 345 nm is abbreviated "E345"; the UV Index is abbreviated "UVI". Trends are provided as "percental change per decade" [% d^{-1}]. Significant trends are printed bold face. n is the number of years used in the trend analysis.

Quantity	Correction Method	n	T [% d^{-1}]	$u(T)$ [% d^{-1}]	$u_U(T)$ [% d^{-1}]	$u_G(T)$ [% d^{-1}]	$u_S(T)$ [% d^{-1}]	$R_U(T)$ [%]	$R_G(T)$ [%]
				February					
E345	1	19	−0.6	3.3	2.5	3.2	–	57	92
E345	2	19	−0.3	3.5	2.5	3.2	–	51	80
E345	3	19	1.0	4.1	2.5	3.2	–	39	62
E345	4	19	−0.6	3.3	2.5	3.2	–	57	92
UVI	1	19	−2.6	4.1	2.5	3.6	–	38	78
UVI	2	19	−2.4	4.1	2.5	3.6	–	38	75
UVI	3	19	−1.1	4.6	2.6	3.6	1.4	30	61
UVI	4	19	−2.6	4.1	2.5	3.6	–	38	78
Ozone	1	16	1.4	3.4	–	1.4	3.1	–	18
				March					
E345	1	18	0.0	3.2	2.6	0.9	1.7	64	8
E345	2	18	−0.2	3.3	2.6	0.9	1.8	61	7
E345	3	18	1.5	3.4	2.6	0.9	1.9	60	7
E345	4	18	0.6	3.9	2.6	0.9	2.8	44	5
UVI	1	18	−0.9	7.1	2.6	1.2	6.5	13	3
UVI	2	18	−1.0	6.8	2.6	1.2	6.2	15	3
UVI	3	18	0.6	7.0	2.6	1.2	6.4	14	3
UVI	4	18	−0.2	7.0	2.6	1.2	6.4	14	3
Ozone	1	19	1.8	6.3	–	0.2	6.3	–	0
				April					
E345	1	19	−1.3	2.8	2.5	0.4	1.2	79	2
E345	2	19	−1.3	3.0	2.5	0.4	1.6	70	2
E345	3	19	0.5	3.5	2.5	0.4	2.3	53	1
E345	4	19	−0.9	3.0	2.5	0.4	1.6	69	2
UVI	1	19	−3.4	5.0	2.5	0.7	4.2	26	2
UVI	2	19	−3.3	5.0	2.5	0.7	4.2	26	2
UVI	3	19	−1.6	5.8	2.5	0.7	5.2	19	2
UVI	4	19	−2.9	4.8	2.5	0.7	4.0	28	2
Ozone	1	21	2.6	3.1	–	0.1	3.1	–	0
				May					
E345	1	17	1.6	5.7	2.8	0.1	5.0	24	0
E345	2	17	1.5	5.5	2.8	0.1	4.7	26	0
E345	3	17	3.7	4.9	2.8	0.1	4.0	33	0
E345	4	17	3.1	6.3	2.8	0.1	5.6	20	0
UVI	1	17	−0.4	5.9	2.8	0.4	5.2	23	0
UVI	2	17	−0.4	5.7	2.8	0.4	4.9	25	0
UVI	3	17	1.8	6.1	2.9	0.4	5.3	22	0
UVI	4	17	1.2	6.5	2.8	0.4	5.8	19	0
Ozone	1	19	1.8	4.0	–	0.3	4.0	–	0

explained with the dominance of cloud and albedo effects for these months.

Results presented in Sect. 4 have shown that trend estimates depend only weakly on the correction method. I also calculated trends without gap correction and varied the maximum allowed number of missing days per month between 5 and 15. As expected, trend uncertainties without gap correction were larger. Requiring less than 5 missing days per month reduced the number of years available for the trend analysis considerably, and I found that 10 days is the best compromise between the two competing desires of accurately calculating a monthly average while having as many years as possible available for the trend analysis.

Autocorrelation was not taken into account when calculating uncertainties of trends because the Durbin-Watson test did not indicate that measurements of consecutive years are

Table 2. Continued.

Quantity	Correction Method	n	T [% d^{-1}]	$u(T)$ [% d^{-1}]	$u_U(T)$ [% d^{-1}]	$u_G(T)$ [% d^{-1}]	$u_S(T)$ [% d^{-1}]	$R_U(T)$ [%]	$R_G(T)$ [%]
				June					
E345	1	18	−0.3	7.2	2.9	0.5	6.6	16	0
E345	2	18	0.2	7.4	2.9	0.5	6.8	15	0
E345	3	18	2.6	6.5	2.9	0.5	5.8	20	1
E345	4	18	0.1	8.3	2.9	0.5	7.8	12	0
UVI	1	18	−1.8	6.9	2.9	0.3	6.3	17	0
UVI	2	18	−1.3	6.7	2.9	0.3	6.1	18	0
UVI	3	18	1.0	6.4	2.9	0.3	5.6	21	0
UVI	4	18	−1.4	7.5	2.9	0.3	6.9	15	0
Ozone	1	20	2.5	2.7	–	0.2	2.7	–	0
				July					
E345	1	19	−2.6	7.8	2.6	0.6	7.4	11	1
E345	2	19	−2.5	8.1	2.6	0.6	7.6	11	1
E345	3	19	−0.7	7.9	2.6	0.6	7.4	11	1
E345	4	19	−1.3	8.0	2.6	0.6	7.5	11	1
UVI	1	19	−6.2	9.1	2.7	0.7	8.7	8	1
UVI	2	19	−6.1	9.0	2.7	0.7	8.6	9	1
UVI	3	19	−4.4	9.2	2.7	0.7	8.8	8	1
UVI	4	19	−5.0	9.3	2.7	0.7	8.9	8	1
Ozone	1	19	**3.6**	3.3	–	0.1	3.3	–	0
				August					
E345	1	19	0.8	7.8	2.8	0.8	7.3	13	1
E345	2	19	0.9	8.2	2.8	0.8	7.7	12	1
E345	3	19	2.6	8.7	2.8	0.8	8.2	10	1
E345	4	19	2.6	8.1	2.8	0.8	7.5	12	1
UVI	1	19	3.6	7.2	2.8	1.3	6.6	15	3
UVI	2	19	3.7	7.5	2.8	1.3	6.9	14	3
UVI	3	19	5.4	8.0	2.8	1.3	7.4	12	3
UVI	4	19	5.3	7.6	2.8	1.3	6.9	13	3
Ozone	1	19	−0.1	2.9	-	0.1	2.9	–	0
				September					
E345	1	17	−3.1	12.6	3.0	0.5	12.2	6	0
E345	2	17	−2.9	12.4	3.0	0.5	12.0	6	0
E345	3	17	−1.4	12.6	3.0	0.5	12.2	6	0
E345	4	17	−3.0	12.7	3.0	0.5	12.3	5	0
UVI	1	17	−2.7	13.2	3.0	0.8	12.8	5	0
UVI	2	17	−2.4	13.0	3.0	0.9	12.7	5	0
UVI	3	17	−0.9	13.2	3.0	0.8	12.8	5	0
UVI	4	17	−2.5	13.2	3.0	0.8	12.8	5	0
Ozone	1	18	0.5	4.7	–	0.1	4.7	–	0
				October					
E345	1	19	**−13.3**	12.4	2.7	0.8	12.0	5	0
E345	2	19	**−13.4**	12.6	2.7	0.8	12.3	5	0
E345	3	19	−11.4	11.4	2.7	0.8	11.1	6	0
E345	4	19	**−13.7**	12.4	2.7	0.8	12.0	5	0
UVI	1	19	**−13.6**	13.0	2.7	1.4	12.6	4	1
UVI	2	19	**−13.7**	13.2	2.7	1.5	12.8	4	1
UVI	3	19	−11.7	12.2	2.7	1.4	11.8	5	1
UVI	4	19	**−14.1**	13.0	2.7	1.4	12.7	4	1
Ozone	1	17	−0.8	4.5	–	0.2	4.5	–	0

Table 3. Comparisons of trends in the UV Index ($\hat{T}_{\mathrm{UVI}}$) estimated from trends in irradiance at 345 nm (T_{E345}) and trends in ozone ($T_{\mathrm{O_3}}$) with trends in the UV Index determined from direct measurements (T_{UVI}).

Month	$\overline{\mathrm{SZA}}$	$\overline{\mathrm{O_3}}$	RAF	Decadal Trend [%]			
	[degree]	[DU]		T_{E345}	$T_{\mathrm{O_3}}$	$\hat{T}_{\mathrm{UVI}}$	T_{UVI}
February	84	413	0.6	−0.6	1.4	−1.4	−2.6
March	73	435	0.8	0.6	1.8	−0.8	−0.2
April	61	424	1	−0.9	2.6	−3.5	−2.9
May	52	385	1.1	3.1	1.8	1.1	1.2
June	48	350	1.1	0.1	2.5	−2.7	−1.4
July	50	323	1.2	−1.3	3.6	−5.6	−5
August	58	301	1.1	2.6	−0.1	2.7	5.3
September	69	300	1	−3	0.5	−3.5	−2.5
October	80	319	0.8	−13.7	−0.8	−13.1	−14.1

T_{E345} and T_{UVI} are based on the data set corrected with Method 4. $\overline{\mathrm{SZA}}$ and $\overline{\mathrm{O_3}}$ are the average solar zenith angle and average total ozone column, respectively. RAF is the Radiation Amplification Factor.

autocorrelated. The effect of cycles with periods of longer than one year was not considered. For example, the monthly means of E345 for June (Fig. 2) appear to be cyclical with a periodicity of 6 yr. If such periodicity had been considered (for example by adding a harmonic function to the linear regression model of Eq. 1), trend uncertainties would be smaller.

The correction factors of Methods 2–4 were determined from clear sky data. Some systematic errors of the instrument such as the cosine error depend on sky condition. The application of correction factors established for clear skies to cloudy conditions is therefore subject to an uncertainty, which was not considered.

6 Conclusions

Trends in monthly average solar irradiance were calculated from spectral UV measurements performed near Barrow, Alaska, between 1991 and 2011. The analysis focused on two quantities: spectral irradiance integrated over the wavelength band of 342.5 to 347.5 nm ("irradiance at 345 nm") and the UV Index. An important objective of this analysis was to quantify the effects of measurement uncertainties and data gaps on the ability to detect statistically significant trends in UV radiation. The method can also be applied to similar environmental data sets. The data set was further tested for systematic errors using radiative transfer calculations, and three different correction schemes to reduce these errors were explored. Depending on the correction method, estimates of decadal trends changed between 1.5 % and 2.9 %. Overall, it can be concluded that systematic errors in the measurements do not play a decisive role in limiting the detectability of trends. Measurement uncertainties have the largest effect on UV irradiance during the spring period when natural variability is small because of large surface albedo.

Trend estimates varied between −14 % and +5 % per decade and were significant (95.45 % confidence level) only for October. Trends for this month varied between −11.4 % and −13.7 % for irradiance at 345 nm and between −11.7 % and −14.1 % for the UV Index. These large negative trends were confirmed with an independent data set of short-wave solar irradiance measured with pyranometers at NOAA's Barrow Observatory and can be explained with a change in snow cover over the observation period: analysis of pyranometer data indicates that the first day of fall when albedo becomes larger than 0.6 after snow fall, and remains above 0.6 for the rest of the winter, has advanced with a statistically significant trend of 13.6 ± 9.7 days per decade. This large trend was derived from a relatively short period (18 yr) and cannot be sustained indefinitely. Trend estimates are sensitive to the first and last point of the time series under consideration. The magnitude of the observed trend may be exaggerated by the fact that the first year of the time series (1992) was the year with the second-earliest onset of snow cover while the last year (2009) was the year with the latest arrival of snow. Trend estimates for longer periods are quite different. For example, the trend for the period 1974–2010 is $+2.7 \pm 3.3$ days per decade and trends for the sub-periods 1974–1991 and 1991–2010 are -6.7 ± 9.0 and $+10.3 \pm 7.6$ days per decade, respectively (Robert Stone, personal communication, NOAA GMD, based on unpublished data, 2011). While it is possible that the timing of persistent snow cover will remain delayed for the foreseeable future as a consequence of climate change, the observed trend could also be a part of a decadal cycle linked to periodic atmospheric circulations (Stone et al., 2005). It can be expected that the large changes in sea ice observed during the last decade will also have a profound influence on precipitation, including timing and amount snow fall.

Trends of total ozone were compared with trends in UV Index, and the two trends were found to be consistent. For ozone, a significant positive trend of 3.6 % was observed for July. Trend estimates for February–June were also positive. These positive trends in total ozone for spring and summer months are consistent with the expectation of the ozone layer's recovery (WMO, 2011), but observations over longer time periods are required to confirm that these trends are sustainable. Results indicate that factors affected by a warming climate, such as snow cover, may affected the future Arctic UV climate more than changes in stratospheric ozone concentrations.

Appendix A

Periods with increased uncertainty

This appendix discusses the reason of outliers seen in Fig. 1, which are indicative of periods with uncertainties larger than those discussed in Sect. 3.2. This analysis is based on Network Operations Reports (available at http://uv.biospherical.com), measurements of the GUV filter radiometer that is collocated with the SUV-100 spectroradiometer (Bernhard et al., 2003), and records of the SUV-100's internal temperature. A more detailed assessment of this information is available at http://uv.biospherical.com/Version2/PaperBAR/Increased_uncertainty.pdf. Periods with increased uncertainty that should not be used for trend analysis are also identified in this document, and data of these periods were excluded from the trend analysis of this paper.

For some months, $q_{\text{monthly}}(y,m)$ is based on less than 10 spectra, indicating long periods of persistent cloudiness. The remaining spectra are likely also somewhat contaminated by clouds and the usefulness of these spectra for QC purposes is questionable. The following discussion focuses on months with at least 10 spectra (solid blue symbols in Fig. 1).

The low values of $q_{\text{monthly}}(1991,7)$ and $q_{\text{monthly}}(1991,8)$ can be explained by the effect of aerosols from the Mt. Pinatubo eruption of May 1991, which may not have been correctly addressed by the model. The low value of $q_{\text{monthly}}(1994,4)$ can likely be attributed to overheating of the instrument.

$q_{\text{monthly}}(2003,7)$ is based on data from the 9, 20, and 21 July only. All other days were cloudy. Solar heating on those days increased the temperature of the instrument's monochromator beyond the capacity of the instrument's thermoelectric cooler. The instrument has a negative temperature coefficient: increased temperatures result in decreased instrument responsivity. Solar measurements are therefore biased low, leading to $q_{\text{monthly}}(2003,7) = 0.91$, which is 6.5 % below $\bar{q}_{\text{monthly}}$. It is not reasonable to correct monthly data upward by this amount, as only three clear-sky days are affected by the temperature effect.

Data from 14 May–31 May 2005 are not available due to a defective instrument shutter; data of May 2005 were not used for trend analysis. The calibration for July 2005 is uncertain and the low value of $q_{\text{monthly}}(2005,7)$ suggest that measurements are indeed biased low.

Calibration scans could not be performed between mid-July and November 2007. The calibration of the instrument for this period therefore has an increased uncertainty. The low values of $q_{\text{monthly}}(2007,8)$ and $q_{\text{monthly}}(2007,9)$ are likely caused by a systematic error in the measurements. The instrument's collector was not cleaned in August 2008, likely leading to reduced responsivity and a low value of $q_{\text{monthly}}(2008,8)$. The instrument was not calibrated in the fall of 2009; data of this period were also not used.

The study of ancillary material could not explain outliers in $q_{\text{monthly}}(y,m)$ for May 1992, March 1993, August 1999, June 2002, and June 2010, indicating that either the measurements of these months are affected by a source of uncertainty that has not been addressed in the uncertainty budget or that the model calculation is biased (e.g. the albedo used in the model might be too small or too large).

Acknowledgements. Between 1991 and 2008, UV measurements used in this study were supported by the National Science Foundation's (NSF) Office of Polar Programs (prime award OPP-0000373) via subcontracts to Biospherical Instruments Inc from Antarctic Support Associates and Raytheon Polar Services Company. Measurements in 2009 were funded by NSF's Small Grants for Exploratory Research (SGER) program (award number ARC-0907819). Measurements of 2010 and 2011 and this study were supported by the NSF Arctic Observing Network program (award number ARC-0856268). I am grateful to the many dedicated individuals who have operated the SUV-100 spectroradiometer at Barrow during the last 20 yr. Upwelling and downwelling shortwave irradiance data were measured by the Global Monitoring Division (GMD) of NOAA's Earth System Research Laboratory and were either acquired from the data archive of the Baseline Surface Radiation Network (BSRN) at http://www.bsrn.awi.de/ or directly obtained from Ellsworth G. Dutton of NOAA/GMD. I thank E. Dutton for preparing a revised pyranometer dataset and for discussing short-wave irradiance data and trends in snow cover. I further thank C. Rocky Booth, James C. Ehramjian, John E. Frederick, and Robert Stone for their valuable comments to the manuscript, and two anonymous reviewers for their valuable suggestions.

Edited by: A. Hofzumahaus

References

ACIA: Arctic Climate Impact Assessment, 1042 pp., Cambridge Univ. Press, New York, 2005.

Bernhard, G., Booth, C. R., and McPeters, R. D.: Calculation of total column ozone from global UV spectra at high latitudes, J. Geophys. Res., 108, 4532, doi:10.1029/2003JD003450, 2003.

Bernhard, G., Booth, C. R., and Ehramjian, J. C.: Version 2 data of the National Science Foundation's Ultraviolet Radiation Mon-

itoring Network: South Pole, J. Geophys. Res., 109, D21207, doi:10.1029/2004JD004937, 2004.

Bernhard, G., Booth, C. R., Ehramjian, J. C., Stone, R., and Dutton, E. G.: Ultraviolet and visible radiation at Barrow, Alaska: Climatology and influencing factors on the basis of version 2 National Science Foundation network data, J. Geophys. Res., 112, D09101, doi:10.1029/2006JD007865, 2007.

Bernhard, G., Booth, C. R., and Ehramjian, J. C.: Comparison of UV irradiance measurements at Summit, Greenland; Barrow, Alaska; and South Pole, Antarctica, Atmos. Chem. Phys., 8, 4799–4810, doi:10.5194/acp-8-4799-2008, 2008.

Booth, C. R. and Madronich S.: Radiation amplification factors: Improved formulation accounts for large increases in ultraviolet radiation associated with Antarctic ozone depletion, in: Ultraviolet Radiation in Antarctica: Measurement and Biological Effects, edited by: Weiler, C. S. and Penhale, P. S., AGU Antarct. Res. Ser., 62, 39–52, 1994.

Blumthaler, M. and Ambach, W.: Solar UVB-albedo of various surfaces, Photochem. Photobiol., 48, 85–88, 1988.

Comiso J. C., Parkinson C. L., Gersten R., and Stock, L.: Accelerated decline in the Arctic sea ice cover, Geophys. Res. Lett., 35, L01703, doi:10.1029/2007GL031972, 2008.

Draper, N. R. and Smith, H.: Applied regression analysis, 3^{rd}edition, 706 pp., John Wiley & Sons Inc., New York, ISBN 0-471-17082-8, 1998.

Dutton, E. G., Farhadi, A., Stone, R. S., Long, C. N., and Nelson, D. W.: Long-term variations in the occurrence and effective solar transmission of clouds as determined from surface-based total irradiance observations, J. Geophys. Res., 109, D03204, doi:10.1029/2003JD003568, 2004.

Dutton, E. G., Nelson, D. W., Stone, R. S., Longenecker, D., Carbaugh, G., Harris, J. M., and Wendell, J.: Decadal variations in surface solar irradiance as observed in a globally remote network, J. Geophys. Res., 111, D19101, doi:10.1029/2005JD006901, 2006.

Gehrke, C., Johanson, U., Callaghan, T. V., Chadwick, D., and Robinson, C. H.: The impact of enhanced ultraviolet-B radiation on litter quality and decomposition processes in Vaccinium leaves from the Subarctic, Oikos, 72, 213–222, 1995.

Gwynn-Jones, D.: Enhanced UV-B radiation and herbivory, in: animal responses to global change in the North, edited by: Hofgaard, A., Ball, J. P., Danell, K., and Callaghan, T. V., Ecol. Bull., 47, 77–83, 1999.

Gurney, K. R.: Evidence for increasing ultraviolet irradiance at Point Barrow, Alaska, Geophys. Res. Lett., 25, 903–906, 1998.

Hessen, D. O. (Ed.): UV Radiation and Arctic Ecosystems, 321 pp., Springer-Verlag, New York, 2001.

Hicke, J. A., Slusser, J., Lantz, K., and Pascual, F. G.: Trends and interannual variability in surface UVB radiation over 8 to 11 years observed across the United States, J. Geophys. Res., 113, D21302, doi:10.1029/2008JD009826, 2008.

Holick, M. F.: Vitamin D deficiency, New. Engl. J. Med., 357, 266–281, 2007.

International Standards Organization (ISO): Guide to the expression of uncertainty in measurement, 101 pp., ISO, Geneva, Switzerland, 1993.

Krotkov, N., Bhartia, P., Herman, J., Fioletov, V., and Kerr, J.: Satellite estimation of spectral surface UV irradiance in the presence of tropospheric aerosols 1. Cloud-free case, J. Geophys. Res., 103, 8779–8793, 1998.

Krotkov, N., Herman, J., Bhartia, P., Fioletov, V., and Ahmad, Z.: Satellite estimation of spectral surface UV irradiance 2. Effects of homogeneous clouds and snow, J. Geophys. Res., 106, 11743–11759, 2001.

Krzyścin, J. W., Sobolewski, P. S., Jarosławski, J., Podgórski, J., and Rajewska-Więch, B.: Erythemal UV observations at Belsk, Poland, in the period 1976–2008: data homogenization, climatology, and trends, Acta Geophys., 59, 155–182, doi:10.2478/s11600-010-0036-3, 2011.

Lenoble, J., Kylling, A., and Smolskaia, I.: Impact of snow cover and topography on ultraviolet irradiance at the alpine station of Briançon, J. Geophys. Res., 109, D16209, doi:10.1029/2004JD004523, 2004.

Lindfors, A. V., Arola, A., Kaurola, J., Taalas, P., and Svenøe, T.: Long-term erythemal UV doses at Sodankylä estimated using total ozone, sunshine duration, and snow depth, J. Geophys. Res., 108, 4518, doi:10.1029/2002JD003325, 2003.

Mayer, B. and Kylling, A.: Technical note: The libRadtran software package for radiative transfer calculations – description and examples of use, Atmos. Chem. Phys., 5, 1855–1877, doi:10.5194/acp-5-1855-2005, 2005.

Maykut G. A. and Church, P. E.: Radiation climate at Barrow, Alaska, 1962–66, J. Appl. Meteorol., 12, 620–628, 1973.

McKinlay, A. F. and Diffey, B. L. (Eds.): A reference action spectrum for ultraviolet induced erythema in human skin, CIE J., 6, 17–22, 1987.

Meehl, G. A., Stocker, T. F., Collins, W. D., Friedlingstein, P., Gaye, A. T., Gregory, J. M., Kitoh, A., Knutti, R., Murphy, J. M., Noda, A., Raper, S. C. B., Watterson, I. G., Weaver, A. J., and Zhao, Z.-C.: Global Climate Projections, in: Climate Change 2007: The Physical Science Basis, Contribution of Working Group I to the Fourth Assessment Report of the Intergovernmental Panel on Climate Change, edited by: Solomon, S., Qin, D., Manning, M., Chen, Z., Marquis, M., Averyt, K. B., Tignor, M., and Miller, H. L., Cambridge University Press, Cambridge, United Kingdom and New York, NY, USA, 2007.

Micheletti, M. I., Piacentini, R. D., and Madronich, S.: Sensitivity of biologically active UV radiation to stratospheric ozone changes: effects of action spectrum shape and wavelength range, Photochem. Photobiol., 78, 456–461, doi:10.1562/0031-8655(2003)0780456SOBAUR2.0.CO2, 2003.

Moody, S. A., Newsham, K. K., Ayres, P. G., and Paul, N. D.: Variation in the responses of litter and phylloplane fungi to UV-B radiation (290–315 nm), Mycol. Res., 103, 1469–1477, 1999.

Manney, G. L., Santee, M. L., Rex., M., Livesey, N. J., Pitts, M. C., Veefkind, P., Nash, E. R., Wohltmann, I., Lehmann, R., Froidevaux, L., Poole, L. R., Schoeberl, M. R., Haffner, D. P., Davies, J., Dorokhov, V., Gernandt, H., Johnson, B., Kivi, R., Kyrö, E., Larsen, N., Levelt, P. F., Makshtas, A., McElroy, C. T., Nakajima, H., Parrondo, M. C. Tarasick, D. W., von der Gathen, P., Walker, K. A., and Zinoviev, N. S.: Unprecedented Arctic ozone loss in 2011 echoed the Antarctic ozone hole, Nature, 478, 469–475, 2011.

Nichol, S. E., Pfister, G., Bodeker, G. E., McKenzie, R. L., Wood, S. W., and Bernhard, G.: Moderation of cloud reduction of UV in the Antarctic due to high surface albedo, J. Appl. Meteorol., 42, 1174–1183, 2003.

Press, W. H., Flannery, B. P., Teukolsky, S. A., and Vetterling, W. T.:

Numerical recipes: the art of scientific computing, 818 pp., Cambridge University Press, Cambridge, UK, ISBN 0-521-30811-9, 1986.

Rex, M., Salawitch, R. J., Deckelmann, H., von der Gathen, P., Harris, N. R. P., Chipperfield, M. P., Naujokat, B., Reimer, E., Allaart, M., Andersen, S. B., Bevilacqua, R., Braathen, G. O., Claude, H., Davies, J., De Backer, H., Dier, H., Dorokhov, V., Fast, H., Gerding, M., Godin-Beekmann, S., Hoppel, K., Johnson, B., Kyrö, E., Litynska, Z., Moore, D., Nakane, H., Parrondo, M. C., Risley Jr., A. D., Skrivankova, P., Stübi, R., Viatte, P., Yushkov, V., and Zerefos, C.: Arctic winter 2005: Implications for stratospheric ozone loss and climate change, Geophys. Res. Lett., 33, L23808, doi:10.1029/2006GL026731, 2006.

Ricchiazzi, P., Gautier, C., and Lubin, D.: Cloud scattering optical depth and local surface albedo in the Antarctic: simultaneous retrieval using ground-based radiometry, J. Geophys. Res., 100, 21091–21104, 1995.

Serreze, M. C., Holland, M. M., and Stroeve, J.: Perspectives on the Arctic's shrinking sea-ice cover, Science, 315, 1533–1536, doi:10.1126/science.1139426, 2007.

Stephens, M. A.:, EDF Statistics for Goodness of Fit and Some Comparisons, J. Am. Stat. Assoc., 69, 730–737, 1974.

Stone, R. S., Dutton, E. G., Harris, J. M., and Longenecker D.: Earlier spring snowmelt in northern Alaska as an indicator of climate change, J. Geophys. Res., 107, 4089, doi:10.1029/2000JD000286, 2002.

Stone, R., Douglas, D., Belchansky, G., and Drobot, S.: Correlated declines in Pacific Arctic snow and sea ice cover, Arctic Research of the United States, 19, 18–25, 2005.

Tanskanen, A., Lindfors, A., Määttä, A., Krotkov, N., Herman, J., Kaurola, J., Koskela, T., Lakkala, K., Fioletov, V., Bernhard, G., McKenzie, R., Kondo, Y., O'Neill, M., Slaper, H., den Outer, P., Bais, A. F., and Tamminen., J.: Validation of daily erythemal doses from Ozone Monitoring Instrument with ground-based UV measurement data, J. Geophys. Res., 112, D24S44, doi:10.1029/2007JD008830, 2007.

United Nations Environment Programme (UNEP): Environmental effects of ozone depletion and its interactions with climate change: 2010 assessment, 236 pp., UNEP, Nairobi, Kenya, ISBN: ISBN 92-807-2312-X, 2010.

Weatherhead, E. C., Reinsel, G. C., Tiao., G. C., Meng, X.-L., Choi, D., Cheang, W.-K., Keller, T., DeLuisi, J., Wuebbels, D. J., Kerr, J. B., Miller, A. J., Oltmans, S. J., and Frederick, J. E.: Factors affecting the detection of trends: Statistical considerations and applications to environmental data, J. Geophys. Res., 103, 17149–17161, 1998.

World Health Organisation (WHO): Global Solar UV Index: A Practical Guide, 28 pp., ISBN 92-4-159007-6, Geneva, Switzerland, 2002, available at: http://www.unep.org/pdf/Solar_Index_Guide.pdf, 2002.

World Meteorology Organisation (WMO): Report of the WMO-WHO meeting of experts on standardization of UV Indices and their dissemination to the public, Global Atmos. Watch Rep. 127, Geneva, Switzerland, 1998.

World Meteorological Organization (WMO): Scientific assessment of ozone depletion: 2002, Global Ozone Res. Monit. Proj. Rep.. 47, 498 pp., Geneva, Switzerland, 2003.

World Meteorological Organization (WMO): Scientific assessment of ozone depletion: 2006, Global Ozone Res. Monit. Proj. Rep. 50, 572 pp., Geneva, Switzerland, 2007.

World Meteorology Organisation (WMO): Scientific assessment of ozone depletion: 2010, Global Ozone Res. Monit. Proj. Rep. 52, 516 pp., Geneva, Switzerland, 2011.